High-Resolution X-Ray Spectroscopy of Galactic Supernova Remnants

Satoru Katsuda[1], Hiroshi Tsunemi[2]

[1] *RIKEN (The Institute of Physical and Chemical Research), 2-1 Hirosawa, Wako, Saitama 351-0198, Japan*

[2] *Department of Earth and Space Science, Graduate School of Science, Osaka University, 1-1 Machikaneyama, Toyonaka, Osaka, 560-0043, Japan*

Corresponding author: katsuda@crab.riken.jp

Abstract

High-resolution X-ray spectroscopy of Galactic supernova remnants (SNRs), based on grating spectrometers onboard XMM-Newton and Chandra, has been revealing a variety of new astrophysical phenomena. Broadened oxygen lines for a northwestern compact knot in SN 1006 clearly show a high oxygen temperature of ∼300 keV. The high temperature together with a lower electron temperature ($kT_\mathrm{e} \sim 1\,\mathrm{keV}$) can be reasonably interpreted as temperature non-equilibration between electrons and oxygen behind a collisionless shock. An ejecta knot in the Puppis A SNR shows blueshifted line emission by ∼1500 km s^{-1}. The line widths are fairly narrow in contrast to the SN 1006's knot; an upper limit of 0.9 eV is obtained for O VIII Lyα, which translates to an oxygen temperature of $kT_\mathrm{O} < 30\,\mathrm{keV}$. The low temperature suggests that the knot was heated by a reverse shock whose velocity is ∼4 times slower than that of a forward shock. Anomalous intensity ratios in O VII Heα lines, i.e., a stronger forbidden line than a resonance line, is found in a cloud-shock interaction region in Puppis A. The line ratio can be best explained by the charge-exchange emission that should arise at interfaces between the cold/warm clouds and the hot plasma. There are several other targets for which we plan to analyze high-quality grating data prior to the operation of the soft X-ray spectrometer onboard Astro-H.

Keywords: supernova remnants - X-rays - individuals: SN 1006, Puppis A.

1 Introduction

There are many scientific motivations to perform high-resolution X-ray spectroscopy of supernova remnants (SNRs), since the X-ray emission is often dominated by thin thermal emission, namely line emission. For instance, accurate line widths allow us to measure the degree of temperature equilibration between electrons and ions as well as efficiency of particle acceleration. Resolved fine structures of lines give us insight into emission processes. We can also reveal ejecta dynamics and measure abundances in unprecedented detail.

Current challenges are based on grating spectrometers onboard XMM-Newton and Chandra. Both of the grating systems are slitless. Therefore, while they work well for point-like sources or compact extended sources, they are generally not suitable for largely extended sources because off-axis emission along the dispersion direction is detected at wavelength positions shifted with respect to the on-axis source. Most SNRs in the large/small Magellanic clouds are small enough for the gratings, and indeed over 10 papers have been published in literature (e.g., Burrows et al. 2000; Rasmussen et al. 2001; Behar et al. 2001; van der Heyden et al. 2001; 2002; 2003; Flanagan et al. 2004; Kosenko et al. 2008; 2011; Broersen et al. 2011). A problem here is that we can not deduce spatial information, since the grating spectra are integrated for the entire SNR. This causes serious ambiguities of interpretations. Therefore, it is important to observe large Galactic SNRs for spatially-resolved high-resolution spectroscopy. However, in this case, grating spectra suffer from spectral degradation due to the spatial extent of the source. The only solution to this dilemma is to focus on locally bright and compact features in large SNRs. We here review a few successful examples of high-resolution spectroscopy of Galactic SNRs with the XMM-Newton's reflection grating spectrometer (RGS: den Herder et al. 2001). The RGS has a large dispersion angle and is more suitable for extended sources than Chandra's grating spectrometer, although there are some nice results (Lazendic et al. 2006; Rutherford et al. 2013).

2 Fast-Moving Knots in SN 1006 and Puppis A

A pioneering work employing the RGS to obtain high-resolution spectra from Galactic SNRs was given by Vink et al. (2003) who observed a northwestern (NW) knot in SN 1006 (see Fig. 1 (a)). As shown in Fig. 1

(b), the RGS spectrum showed several emission lines, including O VII Heα forbidden and resonance, from the knot. By taking account of the degradation effect due to spatial extent, Vink et al. (2003) found intrinsic broadening of O K-shell lines to be $\sigma = 3.4 \pm 0.5\,\mathrm{eV}$. This value was later revised by the same group based on additional deep observations to $\sigma = 2.4 \pm 0.3\,\mathrm{eV}$ (Broersen et al. 2013). The amount of broadening corresponds to an oxygen temperature of $275^{+72}_{-63}\,\mathrm{keV}$, if attributed to thermal Doppler broadening. On the other hand, the electron temperature is derived to be $\sim 1.35\,\mathrm{keV}$, which is ~ 200 times lower than the oxygen temperature. This temperature discrepancy is the evidence for temperature non-equilibration as is expected behind collisionless shocks; the ion temperatures (kT_i) immediately behind collisionless shocks are given by $kT_i = 3/16\,m_i v_{\mathrm{sh}}^2$, where m_i is an elemental mass and v_{sh} is a shock speed, so that the initial temperatures are proportional to particle masses.
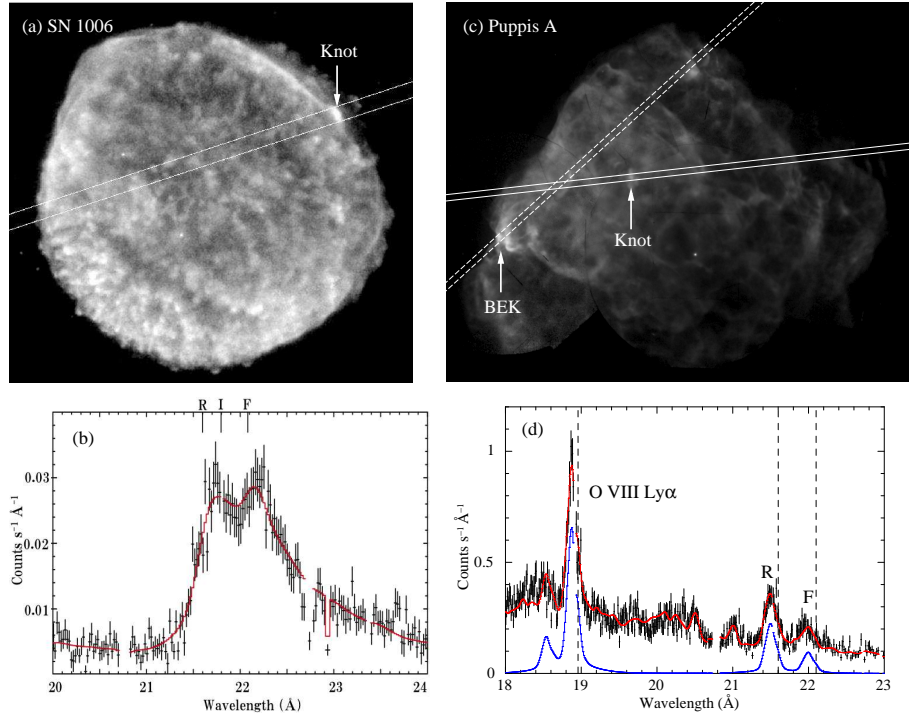
Figure 1: (a) X-ray view of SN 1006 in 500–599 eV, taken from Broersen et al. (2013). The RGS field of view is within the two lines. (b) RGS spectra zooming into O VII Heα from the NW knot in SN 1006. The positions of the resonance (21.6Å), the intercombination (21.8Å), and the forbidden line (22.1Å) are indicated. This figure is taken from Broersen et al. (2013). (c) X-ray view of the Puppis A SNR in 0.5–5 keV. The RGS spectra taken from the two solid lines (hosting the knot) or dashed lines (hosting the BEK) are shown in Fig. 1 (d) and Fig. 3, respectively. (d) RGS spectrum zooming into O K-shell lines from the ejecta knot in Puppis A. In the model, the contribution from the knot is indicated as a blue line. Rest-frame positions of the O VIII Lyα (18.9Å) and the O VII Heα lines are indicated as dashed lines. The blueshifts are clearly visible.

Along the same line, another interesting target is an ejecta knot in the northeast of the Puppis A SNR (see, Fig. 1 (c)) whose southern portion is positionally coincident with an optical O-rich filament (the so-called Ω filament which is not shown here: Winkler & Kirshner 1985). Based on nondispersive X-ray CCDs onboard XMM-Newton (EPIC: Turner et al. 2001, Strüder et al. 2001), Katsuda et al. (2008) noticed blueshifted K-shell lines from the knot. However, the poor energy resolution of the EPIC data ($E/\Delta E \sim 20$) prevented them from conclusive arguments; the Doppler velocity ranged from $1700^{+700}_{-800}\,\mathrm{km\,s^{-1}}$ at the south of the knot, which agrees with the optical measurement of $\sim 1500\,\mathrm{km\,s^{-1}}$ (Winkler & Kirshner 1985), to $3400^{+1000}_{-800}\,\mathrm{km\,s^{-1}}$ at the north of the knot.

Since the knot is bright and compact (~ 5 times brighter than its surroundings and the size is smaller than $\sim 3'$), the RGS is capable of yielding a high-resolution spectrum at a level of $E/\Delta E \sim 150$. Thus, we performed a new XMM-Newton observation, and ob-

tained a nice RGS spectrum as shown in Fig. 1 (d). It exhibits prominent K-shell lines, including O VII Heα and O VIII Lyα. The lines are clearly blueshifted by $1480\pm140\pm60\,\mathrm{km\,s^{-1}}$ (the first and second term errors are measurement and calibration uncertainties, respectively), which is fully consistent with optical measurements for the Ω filament. It is also found that Doppler velocities are uniform within the knot (Katsuda et al. 2013b).

In addition, the RGS spectra enabled us to measure line broadening to be $\sigma < 0.9\,\mathrm{eV}$ at O VIII Lyα, indicating an upper limit of an oxygen temperature of 30 keV. Interestingly, the temperature for Puppis A's knot is at least an order-of-magnitude lower than that for SN 1006's knot, even though they are comparably fast moving.

To interpret the dramatic difference in oxygen temperatures between SN 1006's knot and Puppis A's knot, we investigate temperature equilibration through Coulomb interactions behind collisionless shocks. In the calculation, we assume elemental abundances and the ionization timescales given in the literature (Table 1 in Broersen et al. 2013 for SN 1006 and Table 2's Case-B in Katsuda et al. 2013b for Puppis A). Also, since the degree of electron heating at collisionless shocks is not yet understood well, we examined various initial electron-to-proton temperature ratios, $T_{\mathrm{e}}/T_{\mathrm{p}} = \beta$, for each shock speed. In this way, we ran calculations for several shock speeds. Figure 2 shows the best-representative models, where temperature curves are illustrated only for electrons (black) and oxygen (red). For comparison, we also show model curves with $\beta = m_{\mathrm{e}}/m_{\mathrm{p}}$. We find that the data require fairly different shock speeds; a fast ($\sim$3000 km s^{-1}) shock for SN 1006 and a relatively slow ($\sim$600 km s^{-1}) shock for Puppis A. Also, the values of β are obtained to be $\sim$0.06 for SN 1006 and less

than $\sim$0.5 for Puppis A. These values roughly agree with an observational trend shown in van Adelsberg et al. (2008). Furthermore, the value for SN 1006 is consistent with a direct measurement from Hα spectroscopy for the optical filament ($\beta < 0.07$: Ghavamian et al. 2002). On the other hand, it is interesting to note that our best-estimated value of 0.06 is higher than a recent theoretical prediction, $\beta = 0.023$ for $v_{\mathrm{sh}} > 1500\,\mathrm{km\,s^{-1}}$ (Ohira & Takahara 2008). We will revisit this issue in our future work.

The inferred shock velocity for SN 1006 is roughly consistent with the proper motion of the shock ahead of the knot (Winkler et al. 2003; Katsuda et al. 2013a). Therefore, a simple interpretation is that the knot was heated by a forward shock. However, we cannot rule out a possibility of reverse-shock heating. In fact, the knot shows an elevated Si abundance, suggesting that it originates from the SN ejecta that should have been heated by a reverse shock. In this case, the (reverse) shock velocity should be higher than $\sim$5000 km s^{-1} (see, the discussion in Katsuda et al. 2013b). Such a fast shock requires an oxygen temperature of $\sim$800 keV. This is significantly higher than the X-ray measurement, thereby a significant fraction of the shock energy may go into cosmic-rays. If true, this suggests efficient cosmic-ray acceleration at the reverse shock.

As for Puppis A, the inferred shock velocity, $\sim$600 km s^{-1}, is less than the shocked-gas velocity, $\sim$2000 km s^{-1}, derived by the Doppler velocity of $\sim$1500 km s^{-1} and the optical proper motion of $\sim$1250 km s^{-1} at a distance of 2.2 kpc (Winkler et al. 1988). This is consistent with a picture that the ejecta knot was heated by a reverse shock rather than a forward shock, since the forward shock velocity should be $\sim$2700 km s^{-1} ($= 4/3 \times 2000$ km s^{-1} according to the Rankine-Hugoniot relation).
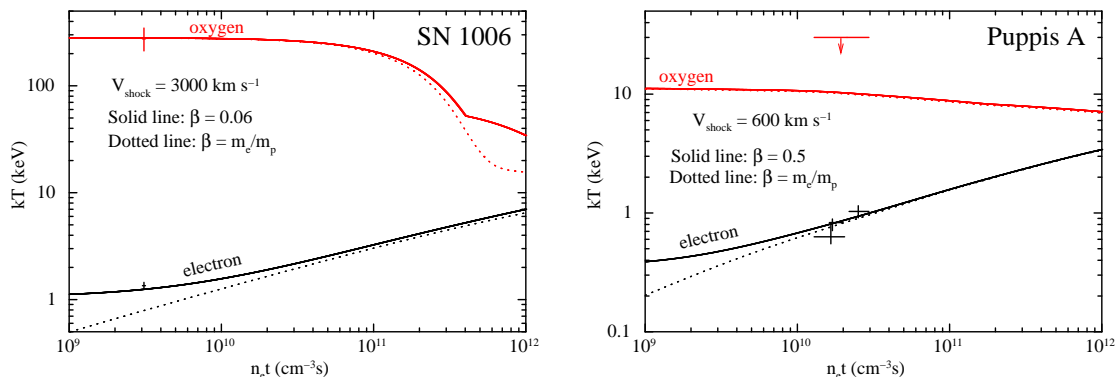
Figure 2: Temperature histories for electrons (black) and oxygen (red) as a function of $n_{\mathrm{e}}t$. Left and right panels are for the NW knot in SN 1006 and the ejecta knot in Puppis A, respectively.

3 Cloud-Shock Interaction Regions in Puppis A

Possible sites for high-resolution spectroscopy of Galactic SNRs are not only ejecta knots but also swept-up ISM regions. In particular, cloud-shock interaction regions in the Puppis A SNR are promising, because they are bright and compact (e.g., Hwang et al. 2005). So far, RGS spectra taken from the bright eastern knot (BEK) and the northern knot were presented by Katsuda et al. (2012). In Fig. 3, we show one of the BEK spectra focusing on the O VII Heα lines, which was taken from the region within the dashed lines in Fig. 1 (c). Interestingly, we see a strong forbidden line with respect to the resonance line. This is inconsistent with any thermal emission models with reasonable plasma parameters (i.e., $kT_e = 0.3$–$0.7\,\mathrm{keV}$ and $n_e t = 10^{10}$–$5 \times 10^{11}\,\mathrm{cm^{-3}\,s}$). After considering a few possibilities to reproduce the anomalous line ratio, Katsuda et al. (2012) proposed that the charge-exchange emission, that arises at interfaces between the cold/warm clouds and the hot plasma, can best explain the data. This would support a long-standing expectation of charge-exchange X-ray emission in SNRs.
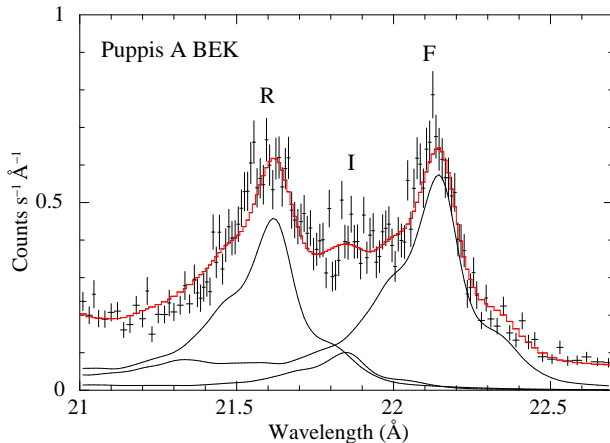
Figure 3: RGS spectrum zooming into O VII Heα from the BEK in Puppis A. The positions of the resonance (21.6Å), the intercombination (21.8Å), and the forbidden line (22.1Å) are indicated.

4 Future Prospects

There are several nice RGS data sets of Galactic SNRs that are waiting for being analyzed. These include bright shells of RCW 86, an equatorial belt in G292.0+1.8, and a southwestern knot in the Cygnus Loop. In addition, it is worth while to search for other promising targets and observe them. We are planning to analyze the RGS data in the near future. The RGS-based study is a great pathfinder for the coming high-

resolution X-ray spectroscopy of SNRs with the non-dispersive soft X-ray spectrometer (Mitsuda et al. 2010) onboard Astro-H (Takahashi et al. 2012).

References

[1] Behar, E., et al. 2001, A&A, 365, L242

[2] Broersen, S., et al. 2011, A&A, 535, 11

[3] Broersen, S., et al. 2013, A&A, 552, 9

[4] Burrows, D. N., et al. 2000, ApJ, 543, L149
doi:10.1086/317271

[5] den Herder, J. W., et al. 2001, A&A, 365, L7

[6] Flanagan, K. A., et al. 2004, ApJ, 605, 230
doi:10.1086/382145

[7] Ghavamian, P., et al. 2002, ApJ, 572, 888
doi:10.1086/340437

[8] Hwang, U., et al. 2005, ApJ, 635, 355
doi:10.1086/497298

[9] Katsuda, S., et al. 2008, ApJ, 678, 297
doi:10.1086/586891

[10] Katsuda, S., et al. 2012, ApJ, 756, 49
doi:10.1088/0004-637X/756/1/49

[11] Katsuda, S., et al. 2013a, ApJ, 763, 85
doi:10.1088/0004-637X/763/2/85

[12] Katsuda, S., et al. 2013b, ApJ, 768, 182
doi:10.1088/0004-637X/768/2/182

[13] Kosenko, D., et al. 2008, A&A, 490, 223

[14] Kosenko, D., et al. 2011, A&A, 532, 114

[15] Lazendic, J. S., et al. 2006, ApJ, 651, 250
doi:10.1086/507481

[16] Mitsuda, K., et al. 2010, SPIE, 7732, 773211

[17] Ohira, Y., & Takahara, F. 2008, ApJ, 688, 320
doi:10.1086/592182

[18] Rasmussen, A. P., et al. 2001, A&A, 365, L231

[19] Rutherford, J., et al. 2013, ApJ, 769, 64
doi:10.1088/0004-637X/769/1/64

[20] Strüder, L., et al. 2001, A&A, 365, L18

[21] Takahashi, T., et al. 2012, SPIE, 8443, 84431Z

[22] Turner, M. J. L., et al. 2001, A&A, 365, L27

[23] van Adelsberg, M., et al. 2008, ApJ, 689, 1089 doi:10.1086/592680

[24] van der Heyden, K. J., et al. 2001,A&A,365,L254

[25] van der Heyden, K. J., et al. 2002,A&A,392,955

[26] van der Heyden, K. J., et al. 2003,A&A,406,141

[27] Vink, J., et al. 2003, ApJ, 587, L31 doi:10.1086/375125

[28] Winkler,P.F. & Kirshner,R.P. 1985,ApJ,299,981

[29] Winkler, P. F., et al. 1988, IAU Colloq. 101: 65

[30] Winkler, P. F., et al. 2003, ApJ, 585, 324 doi:10.1086/345985